Dynamics analysis and GNC design of flexible systems for space debris active removal

Riccardo Benvenuto*, Samuele Salvi, Michèle Lavagna

Politecnico di Milano, Dipartimento di Scienze e Tecnologie Aerospaziali, Italy

Received 23 June 2014
Received in revised form
16 December 2014
Accepted 14 January 2015
Available online 31 January 2015

1. Introduction

Space debris mitigation and remediation are urgent and growing issues to be faced for future space operations and space exploitation durability, especially in Low Earth Orbits (LEO). In the past five decades, several launches have placed more than 5000 satellites into orbit, of which less than a thousand are still operational today. Studies show that for a future continued use of LEO, five to ten strategically chosen and large debris need to be removed every year [1].

The Active debris removal (ADR) topic focuses on trading-off, designing and making operational mechanisms placed on board an active chaser that can rendezvous with and grapple an inert and tumbling target, to eventually change its dynamics either directly transferring it to a graveyard orbit or providing a control device to be attached to the dead element to make it controlled up to disposal. Different techniques have been proposed starting from conventional robotic arms to grasp the target or flexible tethered-nets/tentacles to wrap it, up to action–reaction principle exploitation with no contact at all, such as gas plume impinging on the object surfaces to change its momentum [2].

A general-purpose removal system design should effectively intervene on objects different in configuration, materials and possibly in dimensions such as fragments, entire/parts of dismissed satellites and third stages/fairing elements. Moreover, targets to be captured do not cooperate and have a complex, free, not completely known dynamics. For these reasons, techniques based on capturing debris from a safety distance through the use of thrown-nets seem to be preferable [3]. In contrast with rigid capture mechanisms and traditional docking devices [4,5] these solutions are characterized by passive angular momentum damping and by establishing a tethered connection between the chaser and the target. Furthermore, teleoperation to support the aforementioned scenario activities from ground, is actually not a well suited solution, because of the intermittence, and lack of timeliness in reaction. Autonomous on-board operations would better answer the requirements: that opens new challenges for Guidance, Navigation and Control (GNC) design, especially

* Corresponding author.
E-mail addresses: riccardo.benvenuto@polimi.it (R. Benvenuto), samuele.salvi@mail.polimi.it (S. Salvi), michelle.lavagna@polimi.it (M. Lavagna).

whenever flexible connections are involved in the composite. The chaser GNC system is required to be precise enough to gain stabilized specific relative orbits and to robustly perform de-orbiting operations, while controlling a complex system and damping vibrations of flexible elements and connections.

Research is currently on going at Politecnico di Milano – Department of Aerospace Science and Technologies (PoliMi-DAST) – to design such a tethered-net system for ADR. The problem has been deeply analyzed: a multi-body dynamics simulation tool has been developed to faithfully simulate the net deployment, contact and closure dynamics on the target and the disposal dynamics exploiting the connecting towing tether. This paper, via numerical results, shows that tethered-net systems are a promising technology to capture and remove space debris and discusses the main difficulties that are likely to take place during the towing, particularly from a GNC point of view. The tethered-net dynamics are explored using a discretized viscoelastic tether model. The spatial motion of the system is studied in the Earth gravity field, under the action of the chaser de-orbiting thrusters, for post-capture phases.

Performances, safety and costs of such a de-orbiting mission are presented: influences of relative states and tethered-net design parameters on the system dynamic behavior and controllability are studied. Finally, the case of large space debris removal from the orbit to the Earth's surface is presented, being significant for such a technology.

2. Active debris removal by means of tethered-nets

Flexible ADR/servicing solutions such as throw-nets were studied in the past decade by Astrium from a systemic point of view, as a part of the ROGER study [6], and they have recently been the topic of an ESA CDF study [7]: the space debris issue is, in fact, currently being tackled by the Clean Space initiative[1] at the European Space Agency.

A throw net is cast by impulsively accelerating some flying weights, hereinafter named bullets, attached to the net mouth; then the relative trajectory of the bullets deploys the capture net gradually during the flying process, as shown in Fig. 1. Such a solution is safer than a contact-based mechanism, and applicable to a quite large class of differently shaped objects. By contrast with rigid capture mechanisms, a flexible tethered-net system allows a larger capture distance between the target and the chaser, lowering the collision occurrence chance; it also allows the conversion of a point-to-point capture into a surface-to-point capture, reducing both the capture precision requirements and the stress concentration; it is lightweight, with a quite limited volume demand on board, giving room for multiple captures and disposals within the same flight campaign.

The high system deformability is the price to pay: the system may be complex to control; critical oscillations may rise as rigid connection is no more provided between the target and the chaser; actual net-debris contact prediction is rough and the real contact forces distribution is actually unknown till the connection occurs; some critical operations (e.g. tether deployment) exist and failures management may reveal quite complex.

The closure of the net around the target can occur through free entanglement or through a controlled embedded closing device designed and installed directly on the net frontal opening edge, where winches are placed to retrieve closing strings when commanded, as shown in following simulation examples, where a net closing around an object and exploiting such built-in closing mechanism is presented. A closing device would assure a firmer grasping than the closure relying on wrapping and entanglement, avoiding slippage and limiting the risk of failure during the thrusting phase.

The relative navigation can be performed on board during all the targeting, deployment and impacting phases. Accuracy in the state knowledge is not stringent but needed to tag the epoch for the ejection and the pulling phases at initial instant. Information on the relative position and the relative attitude needed to correctly tag the net release epoch, which affects the evolution of the net dynamics, and capture phases are requested with accuracy of the order of 10^1 cm and 10°.

The net dynamic evolution can be monitored through imaging not to nest sensors on the net itself. Attitude\SK (station keeping) implications should be considered to keep the visual sensors aligned with the line of deployment of the net. The constraints of operations to occur with the target in light may apply, depending on the vision sensor selection. Accuracy on the chaser state vector control is limited due to the fact that a docking is avoided. Fine control is required at the ejection of the bullets but can be decoupled from the chaser attitude control. During the deployment and capture phases, the requirements on respecting a safe distance for collision avoidance and keeping the tether slack are the only ones that tightly affect the chaser SK.

The control authority can be kept on board with a closed loop with navigation, although the ground connection is envisaged to open the on-board loop if needed. Control during the disposal has to face:

- the tether flexibility: continuous versus pulsed control has to be traded off, along with the tether elasticity and strength;
- the tether attitude with respect to the chaser, depending on the relative positioning between the tether and the thrusters devoted to manage the disposal phase: their plume must not impinge on the tether during removal operations.

The close proximity operations are analyzed according to the following mission phases:

- rendezvous and approach along track (*V*-bar),
- net casting: bullet ejection and net deployment,
- target capture: net wrapping the target and closing around it,
- removal or De-orbiting: perigee lowering.

The operations sequence, briefly described above, is sketched in Fig. 2: the reference system is the Local Vertical–Local

[1] http://www.esa.int/Our_Activities/Space_Engineering/Clean_Space.

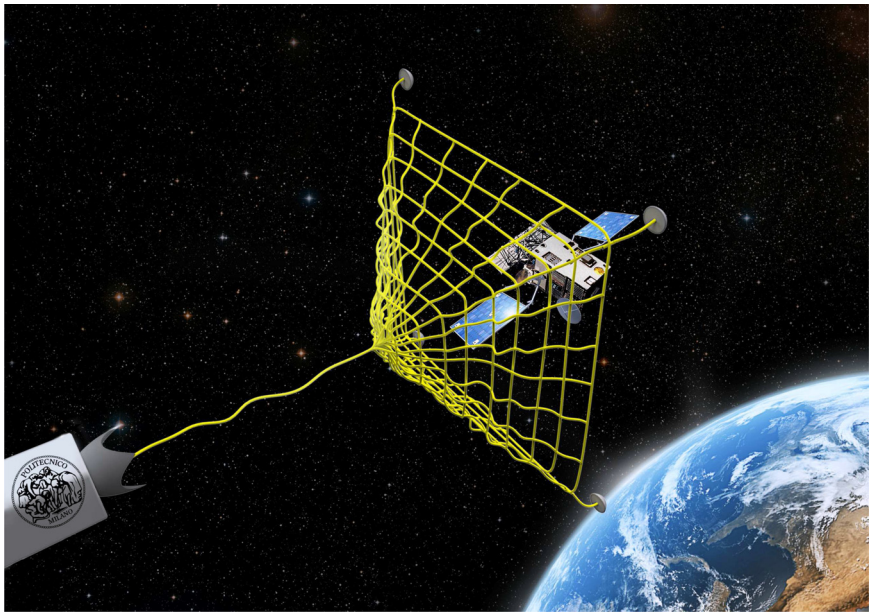

Fig. 1. Illustration of tethered-net concept.

Horizontal frame with *X*-axis aligned with the target velocity direction and *Z*-axis pointing towards Earth.

3. Multibody simulations of flexible ADR systems

To reach a robust GNC design of the net-based solution, a simulator of different phases of removal dynamics is necessary. The tool needs to take into account any flexibility that affects the coupled dynamics due to the presence of flexible devices that are exploited for capture and retention of the debris, such as nets and tethers. As a consequence, the need to resort to a multi-body dynamics approach is evident.

3.1. Modeling the flexibility

Modeling and simulating structures with a high degree of flexibility and involving big displacements, configurations changes (from folded, to deployed, to wrapped), shock loads (the sudden passage of many elements from no load condition to a state of tension) and contact dynamics are extremely challenging tasks. Moreover building a fast and accurate simulator able to rapidly propagate the orbital dynamics of such an object further increases the level of complexity.

Modeling tethers and nets. In terms of modeling tethers and nets, a rigorous approach entails the description of the dynamic behavior by taking into account the effect of flexibility. The deriving equations are Partial Differential Equations (PDEs), depending both on time and spatial coordinates. To solve numerically these differential equations, it is necessary to find a way to transform them into time-dependent Ordinary Differential Equations (ODEs) and solve the equivalent problem. The main solutions to address this issue are the Finite Element Method (FEM), the Assumed Modes Method (AMM) or the lumped-parameters methods. The AMM has proven very effective in describing the transversal and longitudinal vibrations of a flexible structure, relying on shape functions satisfying the boundary conditions of the specific problem. Nonetheless, this kind of approach is generally used if the flexible structures considered are few, e.g. a single tether connecting two sub-satellites or a main satellite with a flexible appendage and a tip mass. With the coexistence of many flexible structures, the problem structuring requires an approach based on simpler methods, always capable of describing the phenomenon, but easier to handle and less costly from the computational time of view. In this sense, with a net made up of hundreds of flexible connections, the AMM seems to be a solution difficult to apply, and this awareness paves the road for the choice of the lumped mass approach. Furthermore, it has been demonstrated [8], how AMM method is numerically unstable with respect to lumped parameters method: simulations are presented using both methods to describe the dynamics of a single orbital tether. Instability arises whenever large configuration changes are made, i.e. during tether release and retrieval. This is particularly important for nets deployment where the passage from folded to deployed entails large configuration changes so that the shape functions are also time dependent, meaning that a complete de-coupling between time and space cannot be obtained. The dynamic modeling of nets has been discussed a lot for fishing applications [9,10]: in these studies it is demonstrated how a lumped parameters method is suitable for describing underwater flexible structures as highlighted by the good agreement with experimental results and how such methods allow treating a wide variety of net configurations and initial conditions with low computational costs and stable solutions.

Generally speaking, a net can be seen as composed by many tethers linked together with knots: in this view, most of the considerations made about tether dynamics modeling are still valid for modeling nets. In multi-body

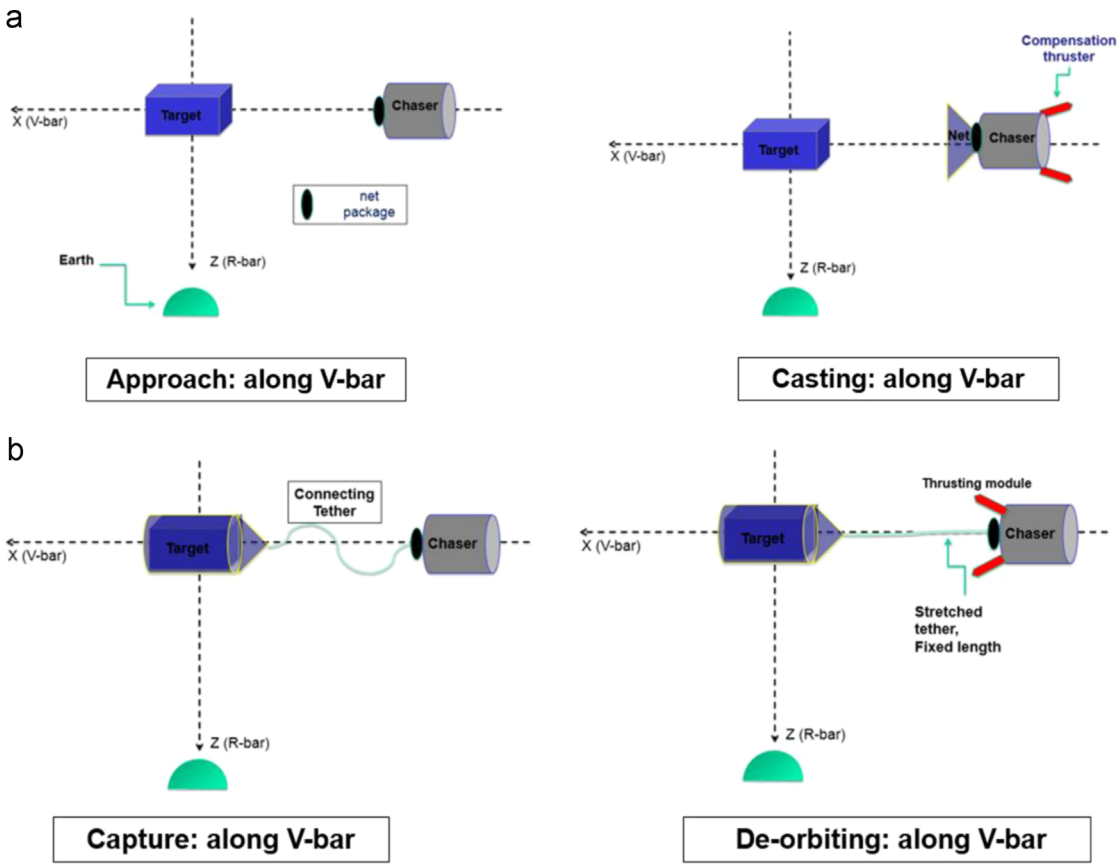

Fig. 2. Representation of mission phases sequence.

dynamics, lumped-parameters methods are widely used, and several studies exist that applies the so-called beads model to space tethers [11,12]. Furthermore, these methods are intrinsically three-dimensional and can automatically take into account tether 3D librations and 3D vibrations. An interesting problem is how to use the discrete models for the simulation of the tether deployment and retrieval. In the case of discrete model, there are two kinds of schemes usually used to deal with variable length tethers [13]. In the first scheme, the tether is represented as a fixed number of elements and the deployment (or retrieval) process is simulated by simultaneously changing the physical properties of all elements. The other scheme involves a variable number of elements, and simulates the deployment (or retrieval) process by only varying the length and mass of the first element and adding an element to (or removing it from) the start of the chain of the elements when certain criteria are met, for instance, the length of the first element exceeding (or reducing below) a predetermined amount. Each of the approaches has its merits for simulating flexible tethers; the first has been chosen here for computational and coding reasons: having a fixed size state vector is more performing from the propagation algorithm point of view.

A flexible body, that does not withstand compression, can be discretized as series of point masses (each having 3 degrees of freedom and null inertia) connected by springs and dashpots. This way the constitutive law of the material can be modeled through the combination of spring-dampers: the law can be user-defined, linear or non-linear, and its parameters can be fixed or variables during forward dynamics integration. The simplest and yet most efficient way to describe the mechanical tension on ropes is the linear Kelvin–Voigt model [14]. A Kelvin–Voigt material is a viscoelastic material having the properties both of elasticity and viscosity: the model can be represented by the mechanical parallel of a purely elastic spring and a purely viscous damper. This model presents several advantages because of its linearity and direct relationship of its coefficients to material mechanical properties; however physical inconsistencies are present and related to the unnatural shock forces at the moment of tug (un-stretched to stretched condition) and to tensile or "sticky" forces at the moment of load removal. This second inconsistency, however, can be overcome by forcing the tension to be null when the tether is slack, as expressed in Eq. (1). Tension on rope elements can be expressed as

$$\boldsymbol{T}_{ij} = \begin{cases} \left[-k_{ij}\left(|\boldsymbol{R}_{ij}| - l_{nom}\right) - d_{ij}\left(\boldsymbol{V}_{ij}\hat{\boldsymbol{R}}_{ij}\right)\right]\hat{\boldsymbol{R}}_{ij} & if\,|\boldsymbol{R}_{ij}| > l_{nom} \\ 0 & if\,|\boldsymbol{R}_{ij}| \le l_{nom} \end{cases} \tag{1}$$

where

- k_{ij} and d_{ij} are the elastic and viscous parameters between elements i and j,

- l_{nom} is the nominal un-stretched length of the tether element,
- $\boldsymbol{R}_{ij}$ and $\boldsymbol{V}_{ij}$ are, respectively, the relative position and velocity between two consecutive masses.

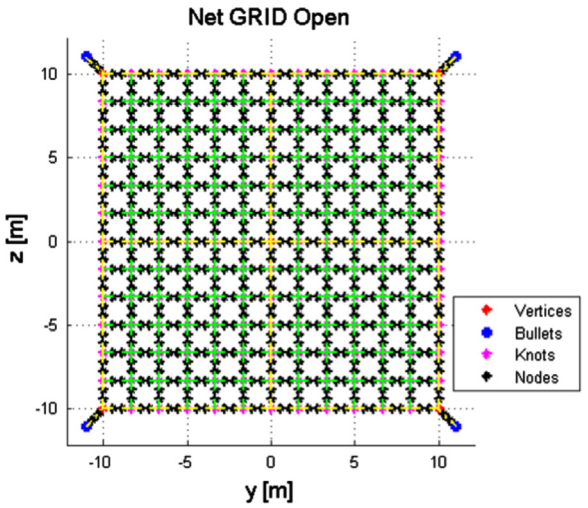

Fig. 3. Discretization of a $20 \times 20\ \mathrm{m}^2$ large meshed net with 2403 degrees of freedom (two nodes per thread).

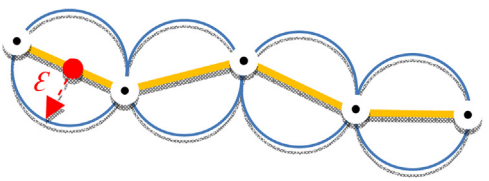

Fig. 4. Discretization of a net thread and spherical bounding boxes exploited for the finest elements.

By using this law the stiffness is directly related to material and rope properties, the axial stiffness being defined as

$$k_{ij} = \frac{EA}{l_{nom}} \tag{2}$$

where E is the Young's modulus and A the thread cross section. The damping is directly related to the tether mass and natural frequency through its damping ratio ξ as in the following equation:

$$d_{ij} = 2\xi\omega_{ij}m_{ij} \tag{3}$$

Damping ratio and Young's Modulus have been determined experimentally at PoliMi-DAST premises for different synthetic fiber ropes that are suitable candidate, meeting the requirements on strength and stiffness.

With such a model, the equation of motion for mass i is given by Newton's second law

$$m_i\frac{d^2\boldsymbol{R_i}}{dt^2} = \boldsymbol{F_{Gi}} + \sum_{j=-1,1} \boldsymbol{T}_{i,i+j} + \boldsymbol{F}_{ext} \tag{4}$$

where

- $\boldsymbol{T}_{i,i+j}$ is the tension between the mass i and $i+j$, as defined in Eq. (1).
- $\boldsymbol{F_{Gi}}$ is the gravitational force.
- $\boldsymbol{F}_{ext}$ is other generic external forces (control, perturbations, etc.).

Each rope composing the net can be discretized in an arbitrary number of elements, as depicted in Fig. 3.

Lumped-parameters methods allow to obtain an explicit system of ODEs: this leads to the possibility of building-up non-recursive algorithms to parallelize the computation and

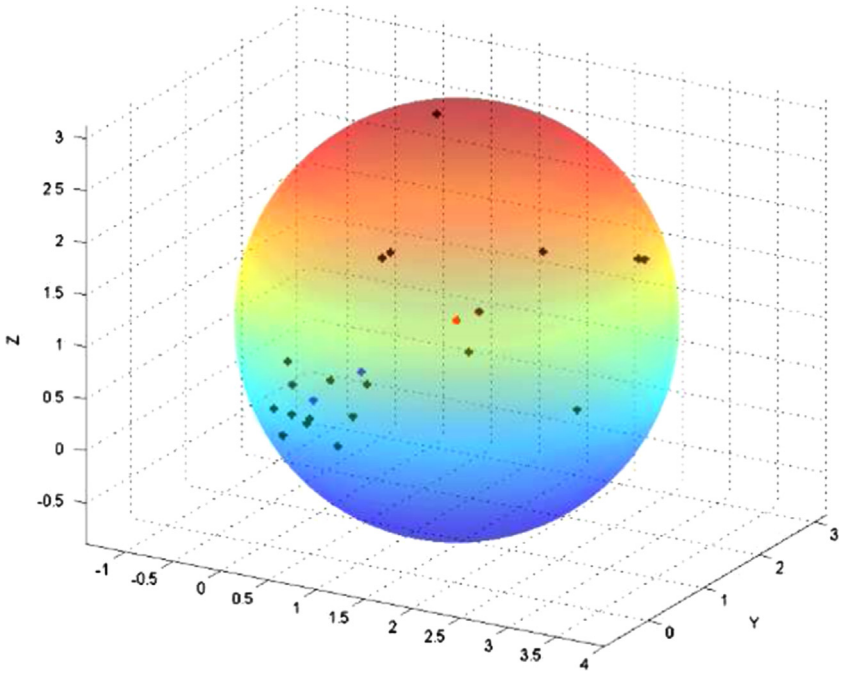

Fig. 5. Example of a Minimum Spherical Bounding Box enclosing a specific subset of points.

speed it up. The choice of integrators depends on the model properties: whenever different stiffness elements are present in the model (for example with different stiffnesses of net and tether or when flexible appendages are included), the problem gets stiff and the one-step adaptive explicit Runge–Kutta method is substituted by a multi-step implicit Runge–Kutta formula with a trapezoidal rule step as first stage and a backward differentiation formula as second step [15]: this method delivers a solution without numerical damping and use crude error tolerances not to excessively slow down computation during high stress conditions and shock loads.

Modeling the end bodies. Chaser, target and bullets are modeled as six degrees of freedom bodies through Newton's and Euler's laws for translational and rotational dynamics. The target in non-cooperative and non-controlled while the chaser can be controlled. All reactions on bodies due to net and tether are taken into account. More details about models and equations of motion are given in Appendix A.

Modeling flexible appendages. The flexibility of appendages, such as solar panels or antennas, also needs to be taken into account for reliable simulations. These flexible beams are modeled as a chain of extended (6 degrees of freedom, non-null inertia) rigid bodies and viscoelastic joints [16]. The joint law can be user-defined and tuned as in the tether case.

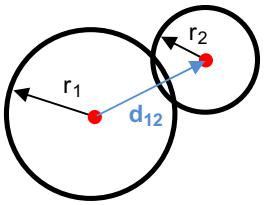

Fig. 6. Representation of the coherence condition between two different Spherical Bounding Boxes.

3.2. Collision detection

To avoid penetration of target thin or protruding elements in the net threads, respecting the physics of the phenomenon, a hierarchical bounding-boxes collision detection algorithm [17,18] has been set-up. It consists of an n-phases algorithm refining the zone of contact, in order to select the specific subsystems of nodes to be cross-checked for collision. This strategy has the main advantage to speed-up the simulation, keeping the same precision. The error (ε) is null in the case of massive nodes, while equal to half of the element length in the case of viscoelastic thread elements.

The control boxes considered are MSBB (Minimum Spherical Bounding Boxes), as shown in Fig. 4. MSBB are built-up as the minimum spherical bounding volumes enclosing a specific subset of nodes [19] Fig. 5.

The nodes to be cross-checked are the net and target ones. Both the collision between net and target and the self-collision among the net threads are resolved. Net relevant points are both the physical knots and the discretizing nodes; they are hierarchically grouped as shown in Fig. 9 (where numbering represents the hierarchy level) [20].

The coherence between two MSBB, meaning their overlap, engages the analysis between the MSBB of the next level in a cascade process. The advantage of using spherical bounding volumes lies in the absolutely minimum computational work required to evaluate the coherence between two subsets of nodes, as it is identified when the distance between their centers is lower than the sum of the radii Fig. 6.

Coherence condition is expressed by the following equation:

$$d_{12} < r_1 + r_2 \tag{5}$$

The same boxes geometry has been chosen for the description of the target mesh, as visible in Fig. 7, since

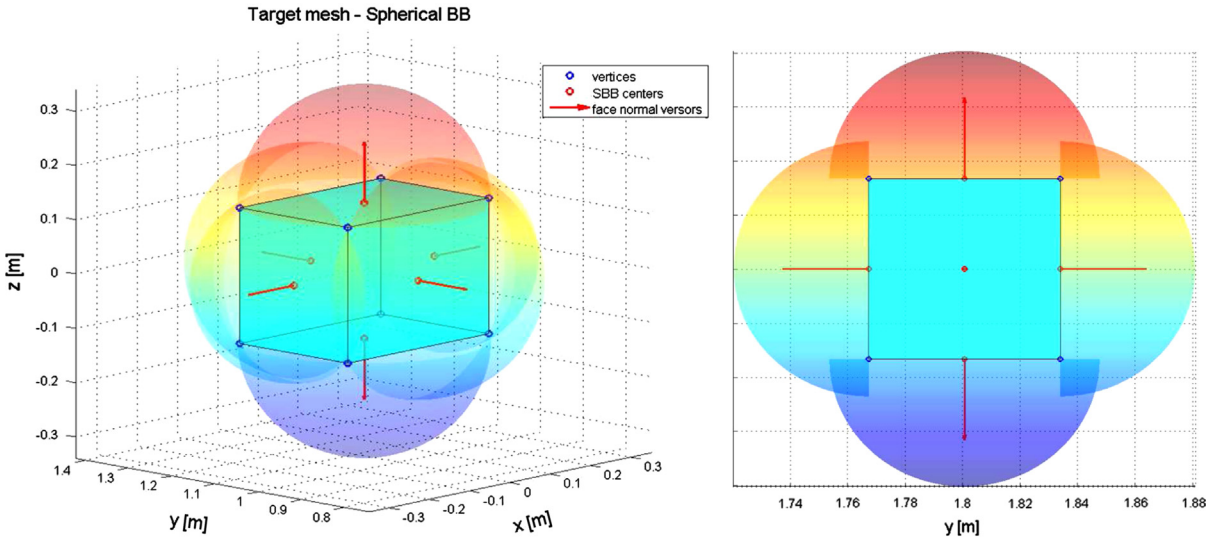

Fig. 7. Target contact mesh using Spherical Bounding Boxes.

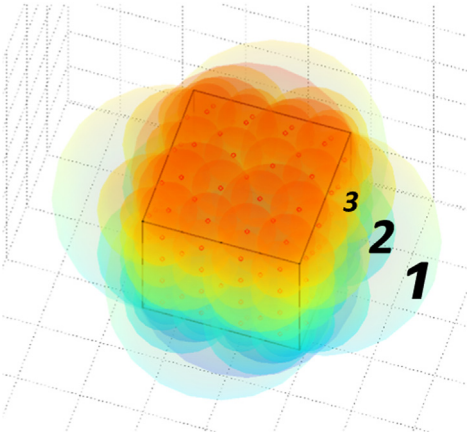

Fig. 8. Target Spherical Bounding Boxes.

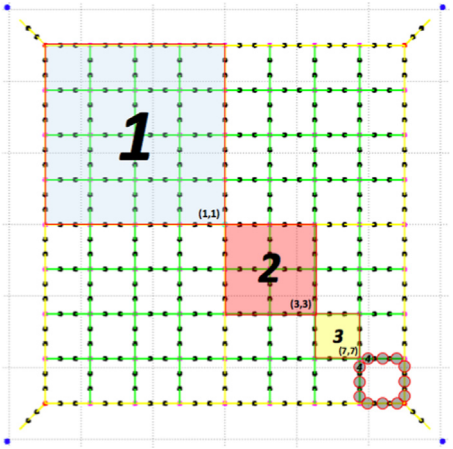

Fig. 9. Net hierarchical sub-division of nodes.

consistency is required between colliding bodies. The nodes to be enclosed in the bounding spheres correspond to the mesh nodes: this allows to build an interface to import arbitrary geometries. Each face is further hierarchically discretized in smaller surface mesh [21] as can be seen in Fig. 8, each represented by its proper MSBB and normal unit vector exiting from the surface.

The impact of a net node on a surface of the target is registered only when both coherence between two spheres occurs and the projection of their distance on the surface exiting unit vector is positive. This is the necessary condition that let to trigger the next step of the contact algorithm. Surface impact coherence conditions are expressed by

$$\begin{cases} d_{12} < r_1 + r_2 \\ d_{12}\hat{n} > 0 \end{cases} \tag{6}$$

where $\hat{n}$ is the surface exiting unit vector. When the latest mesh level is reached, a further check is made considering the surface edges, in order to exactly compute the impact point.

The selected MSBB method allows an easy and extremely precise treatment of the impact of the net with borders and edges, without further check algorithms. At high level, models describing net dynamics and contact dynamics allow to limit the computational time: lumped parameters methods in this view are those offering the least computational effort with an acceptable level of accuracy. Furthermore, the discretization of the net/threads in point masses allows a much faster and simpler management of collision detection and contact algorithms.

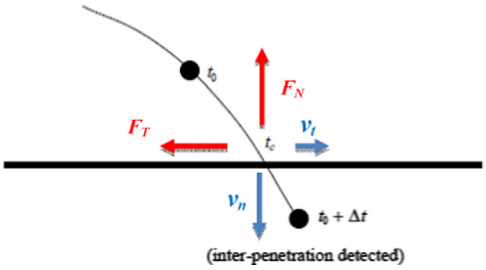

Fig. 10. Contact reaction forces.

3.3. Contact dynamics

The contact dynamics have been treated with the penalty method [22]: the contact is resolved a posteriori, i.e. after it has happened, and the reaction force is proportional to the penetration, called penalty, between the bodies Fig. 10. Such a method allows to keep the same explicit ODE structure of the system. Several models exist for contact dynamics: the linear Hertz law has been chosen, as in Eq. (7), for forces normal to the contact surface. For the tangential forces, a Coulomb friction model has been considered as shown in Eq. (8).

$$F_N = -k_n s_n - c_n v_n \tag{7}$$

$$F_T = -k_C F_N v_t / |v_t| \tag{8}$$

where

- v_n, s_n and v_t are respectively the normal and tangential components of the penetrating velocity and its integral.
- k_n and c_n are tunable coefficients characteristics of the impacting surface and impacting object.
- k_C is the dynamic Coulomb friction coefficient.

Such a method does not account for relaxation time, and a tuning of elastic, damping and friction coefficients through experimental investigation is needed.

3.4. Closing mechanism

A closing mechanism may be mandatory to ensure a successful capture and a safe de-orbit pulling. To ensure the closure of the net a thread ring is introduced at the net mouth and it is wound by winches inside the bullets: these winches are conceived as spring reels automatically activated when the impact is detected. This event-driven control applied to winches has demonstrated, through simulations, to be more reliable than a time-driven control. However a delay between impact detection and closing command, dependent on the target-net geometrical features, is introduced to guarantee the net correct

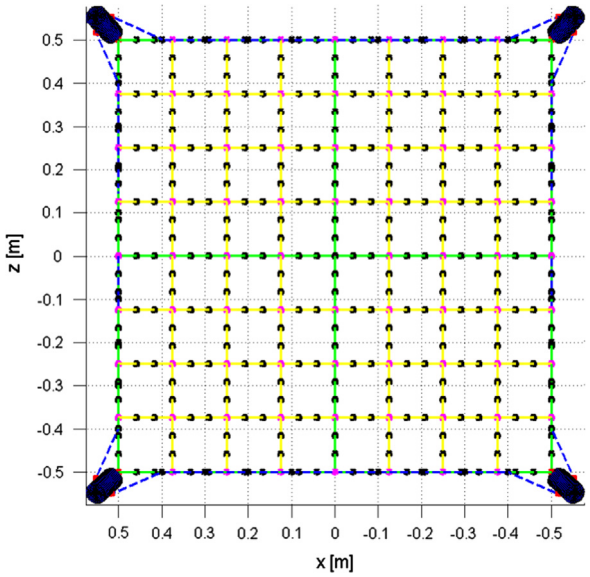

Fig. 11. Interlaced thread closing option.

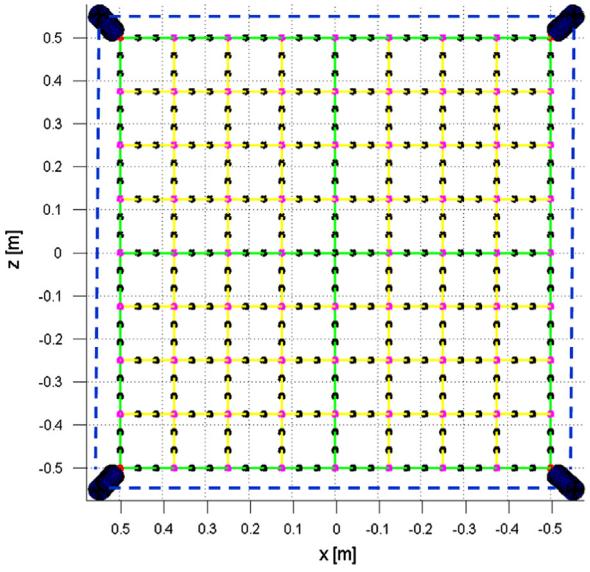

Fig. 12. Free closing links.

closure. The closing thread may be conceived to be interlaced with the net perimeter, such as in Fig. 11, or to be only connected to bullets, as in Fig. 12. In the first case the closing thread is connected to all perimetral knots.

During the closure, the closing links' winding is simulated reducing the nominal length of these links, generating the stress responsible for the closure on the nodes where they are attached. The closing threads are modeled as any other threads except for their variable length: the length can be externally controlled at any time to simulate winding and unwinding. A change in element length leads to a change in stiffness, damping and mass: properties changes of all nodes/elements belonging to the same threads are equally distributed. Each rolled/unrolled thread mass is added/removed to the closer winch's mass (winches are supposed to be contained inside the bullets). Slippage of threads on the knots due to interlacing has not been considered in this work.

Simulation examples of both types are presented hereinafter. A linear control law has been implemented for the closing threads and controlling their length in an event-driven way (the closing law is activated whenever the impact between tether and net is detected).

3.5. Net deployment and capture sequence

A full-scale net deployment and capture dynamics is first presented in Fig. 13: a 30×30 m^2 planar geometry is proposed for a large size target, since wrapping dynamics is necessary for planar shapes. In the simulation the target is rotating at 5° per second around its maximum inertia axis and the net firmly closes around it with an interlaced closing mechanism. Parameters of this simulation are reported in Table 1.

A pyramidal net is also presented for the case of an In-Orbit Demonstration mission (IOD) of such a capturing technique: the target is in this case a CubeSat. 3D geometries are advised whenever a quasi-contactless capture is aimed at, for example with small satellites, or to increase the capture safety and robustness face to the target state. Simulation parameters are listed in Table 2.

The pyramidal net is presented for both the cases of non-interlaced and interlaced closing mechanisms, respectively in Figs. 14 and 15. As it is possible to remark the non-interlaced case does not lead to a complete closure of the net around the target, the closing threads being only attached to bullets: the closed configuration presents a loose perimeter, which does not guarantee a firm and strong grasping of the net, especially during de-orbiting operations. On the other hand the interlaced closing mechanism allows a complete closure of the net, being the closing threads linked to the whole net perimeter. This guarantees a firmer and stronger grasping and a safer capture, reducing slippage between net and target, and by consequence reducing the relative motion of the target inside the net during pulling phases. Furthermore the complete closure of the net also improves the containment features: in case debris are created during capture, this will help to contain them inside the net, which represents and advantage of the net capture system itself. For these reasons the interlaced closing mechanism is the preferred solution in terms of safety and reliability.

4. The removal phase

The following case is of particular interest for ADR and represents a conservative case, being the large size debris de-orbiting. In such a case a controlled re-entry is required. A controlled de-orbiting of a spacecraft from LEO, resulting in an immediate atmospheric re-entry at a predefined position is only feasible with a chemical propulsion system. In order to confine the impact area to a size of few hundred square kilometers, it is necessary to have a sufficiently steep flight path angle at the atmospheric interface. Simulations predicting the destruction of the spacecraft during re-entry [23] and the impact area

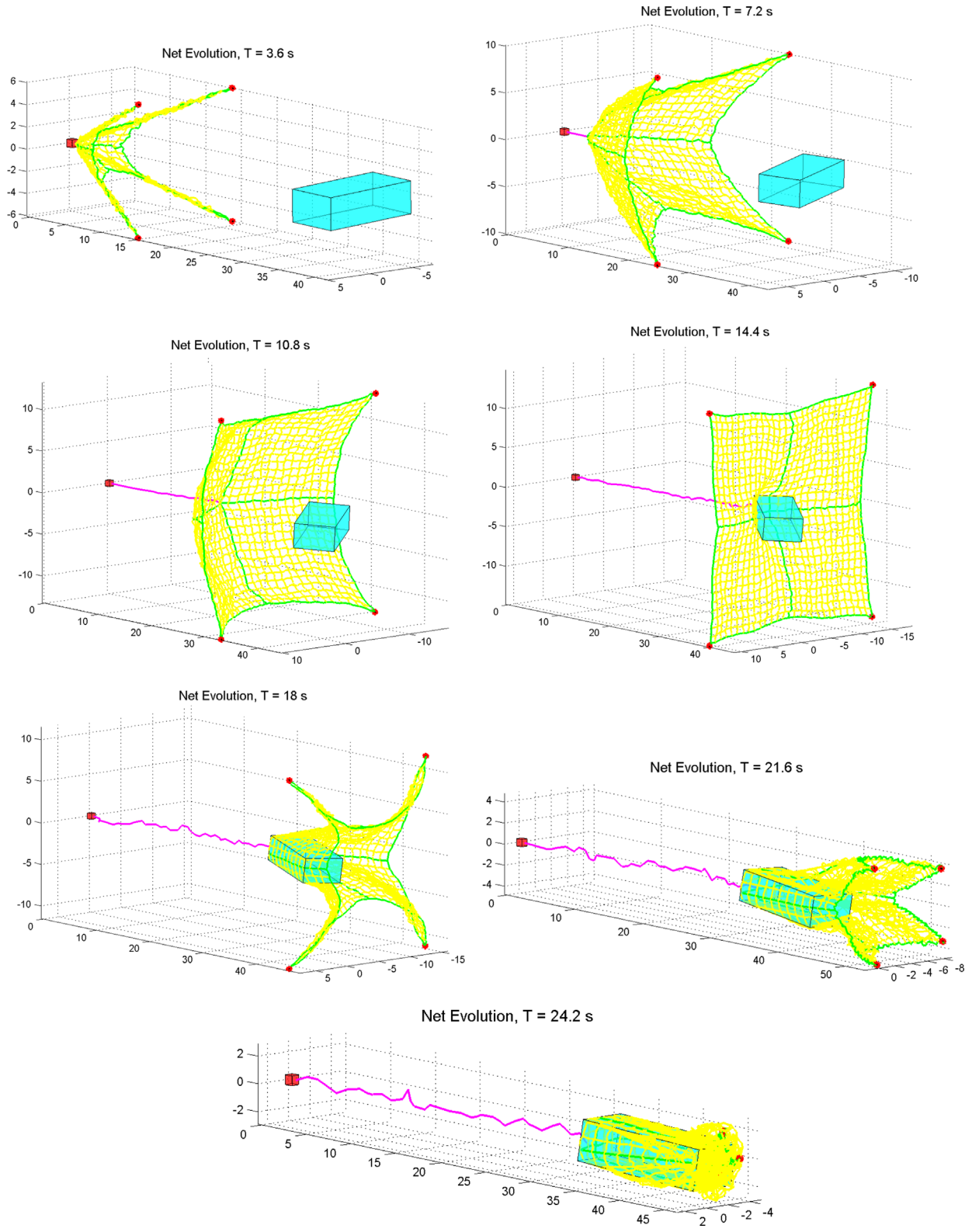

Fig. 13. Planar, interlaced closing mechanism – large size target. Pyramidal net – non-interlaced closing mechanism, Planar net – interlaced closing mechanism.

size have shown that the perigee of the transfer orbit leading to the re-entry has to be 60 km or lower. This requires a flight path angle at the atmospheric interface, defined by convection at 120 km altitude, in the range from -1.5° to -2.5°, depending on the initial orbit altitude. The resulting delta-*V*, required to de-orbit debris from an altitude of 800 km under this flight constraints, is around 200 m/s. By taking into account such constraint, high thrust chemical propulsion has been selected for de-orbiting burns.

The removal phase can be divided into the following sub-phases

- the free motion after capture;
- the tether tensioning phase;
- the propelled phase;
- the post-burn phase.

The duration of free motion after capture is limited as much as possible to avoid the appearance of instabilities that would lead to entanglement and potential failures. Also the ignition of main engines with a slack tether would lead to whiplashes effects and control loss: a tensioning of the tether is then necessary and it is carried out using reaction control systems (RCS), which are supposed to have a thrust two orders of magnitude lower than main engines (a 25 N thrust in 3 axis has been assumed as RCS in this case). Therefore, the RCS are activated at the beginning until a desired level of tether tension is reached, at this point the control switches to high thrust pull. In this way the tether is pre-tensioned before

Table 1
Planar net parameters.

Type	Planar (13107 DOF)
Size (m)	30×30
Mesh (m)	1×1
Mass (kg)	4.269
Bullet Initial Impulse (N)	3.47
Closing time (s)	10
Target size (m)	$5 \times 3 \times 10$
Target angular velocity (deg/s)	5

Table 2
Pyramidal net parameters.

Type	3D-pyramidal (2859 DOF)
Size (m)	1×1
Mesh (m)	0.25×0.17
Mass (kg)	0.716
Bullet Initial Impulse (N)	0.49
Closing time (s)	0.3
Target size (m)	$0.2 \times 0.2 \times 0.6$
Target angular velocity (deg/s)	3

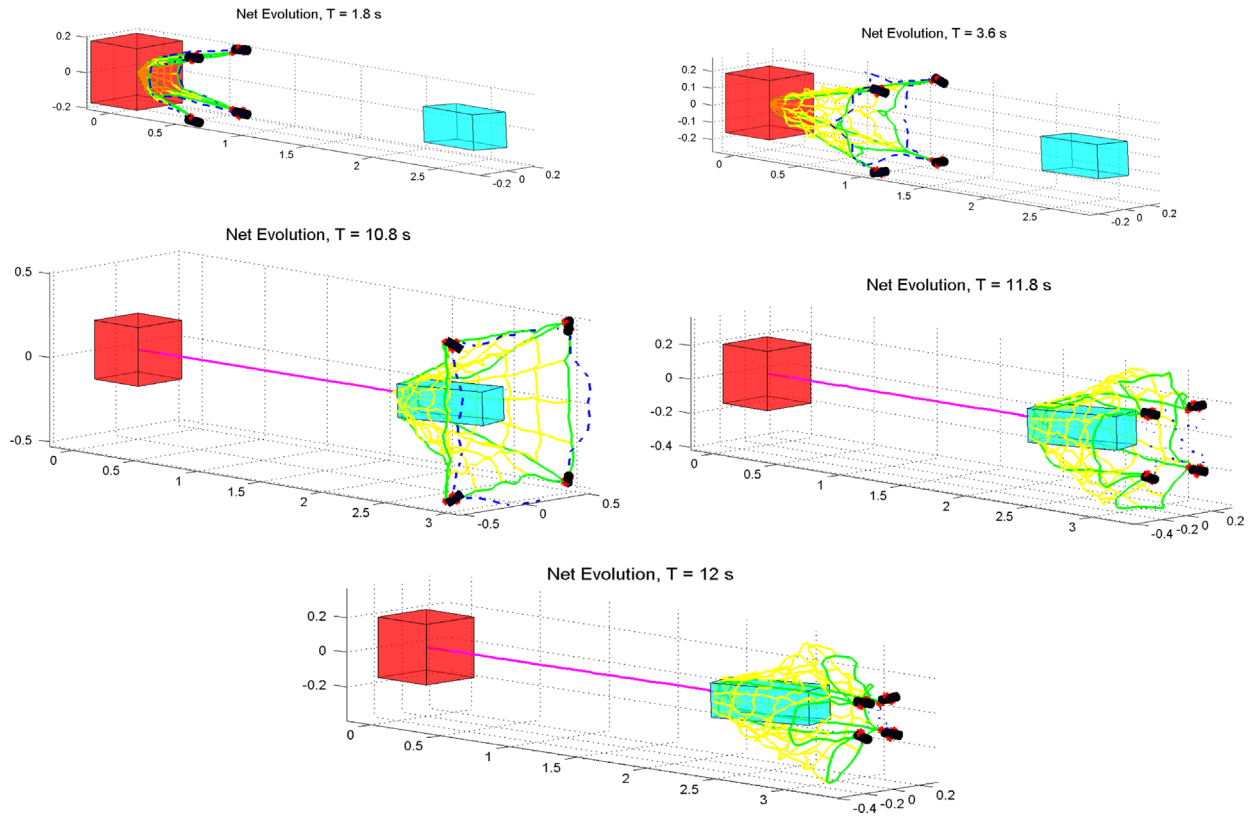

Fig. 14. Pyramidal, non-interlaced closing mechanism – small size target. Pyramidal net – interlaced closing mechanism, Pyramidal net – non-interlaced closing mechanism.

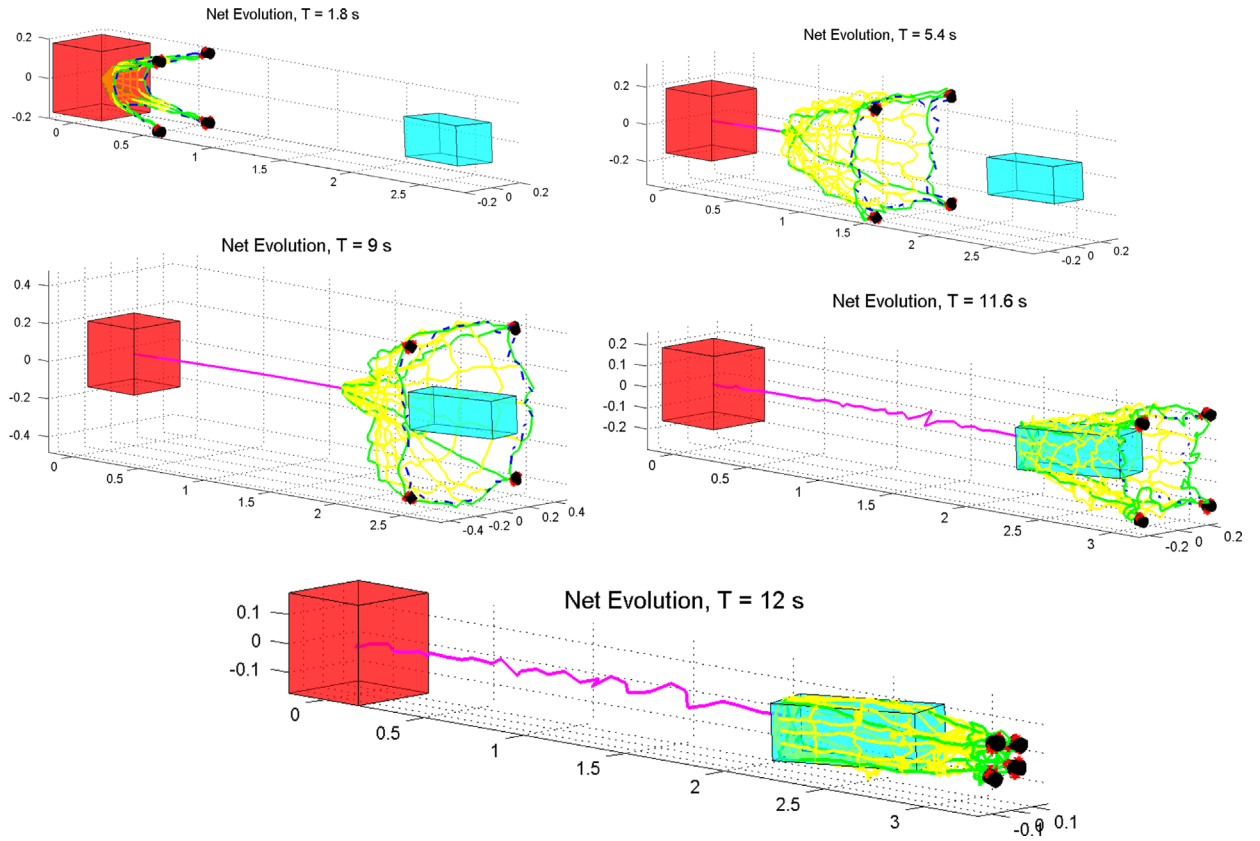

Fig. 15. Pyramidal, interlaced closing mechanism – small size target, Pyramidal net – interlaced closing mechanism.

powering the main engines, to stabilize the system avoiding shock loads and high amplitude oscillation at the ignition of main engines. During the high-thrust propelled phase the chaser needs to be controlled in attitude and position relative to the target and the tether vibrations need to be damped. Finally, the post-burn phase is a crucial part for the success of the mission. After the burn, in fact, the residual tension on the tether makes the two objects moving towards each other, setting them in a collision path. In order to avoid this, several solutions can be considered, the most straightforward being

- to perform a single burn and afterwards cut the tether and perform a collision avoidance maneuver (CAM), leaving the target in the correct re-entry path;
- to synchronize the thrust with the relative motion so that, at the end of a burn, zero relative velocity (corresponding to a minimum of tether tension) between the two craft is achieved; this requires tension sensors on the tether and a fast and accurate control;
- to modulate the thrust cutting off the natural frequencies of the tether and removing the associated energy.

The third option, or thrust shaping, has proven [24] to significantly reduce the post-burn relative motion between the vehicles. However, to the authors' knowledge, no European high-thrust throttling module is currently available. For this reason, the first solution has been considered here. This option is not feasible if a multi-burn strategy is foreseen, on the other hand it is particularly interesting if multiple captures and removals need to be carried out by the same chaser.

Simulations on debris de-orbiting dynamics have run using a simplified model, depicted in Fig. 16. The tether is discretized with 10 lumped masses while the flexible appendages are discretized with 3 elements each. In this way the flexibility of all connection can be taken into account to simulate the de-orbiting dynamics. The system is subjected to gravitational forces and torques: the gravity gradient is considered, being of particular importance for large flexible space systems, as the ones analyzed here.

Here a non-slipping single contact point has been assumed as connection between tether and target, to focus the study on the system sensitivity to physical properties, as tether stiffness or damping. Therefore, the model used in the following simulations is not completely representative of net capturing conditions, the last being characterized by multiple slipping contact points. Nevertheless, this simplified model allows to preliminary size the system, assess the feasibility and synthetize control laws that can later be applied to a refined model to prove their robustness. Simulation parameters are reported in Table 3.

The previous parameters, in particular the thrust level and burn duration, guarantee a flight path angle at 120 km equal to -1.78°, respecting the policy on controlled re-entries. During the burn, chaser attitude is controlled via a

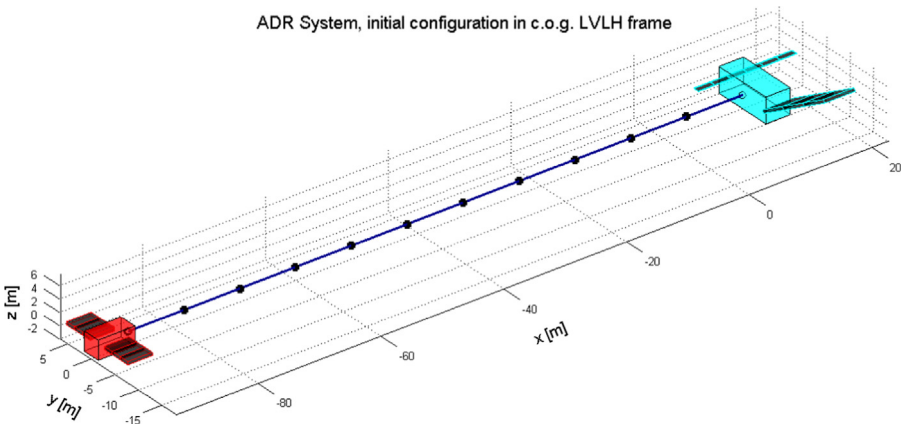

Fig. 16. De-orbiting model (chaser in red, target in cyan).

Table 3
De-orbiting simulations parameters.

Chaser mass (kg)	1300
Target mass (kg)	8000
Initial orbit altitude (km)	800 (LEO)
Thrust (N)	2×1000
Burn duration (s)	920
Tether length (m)	102

Table 4
Simulation parameters – tether stiffness.

Case	**Stiffness (N/m)**
Stiff	1.57e3
Non-stiff	1.57e1

simple PID controller: the chaser attitude is controlled to keep the thrust aligned as much as possible with the anti-velocity direction to maximize the transfer efficiency. This also prevents the system to drift towards the radial direction, as it would tend to do in free motion. The tether is pre-tensioned to a value of 50 N through attitude thrusters and then the high thrust engines are turned on to perform de-orbiting: as previously mentioned, this is carried out to avoid an initial high shock load on the tether. The high-thrust module is here simply controlled with a switch.

4.1. Stiff versus non-stiff elastic tether

Simulations examples are presented for two different tether materials, the tether length and cross area being the same: a stiff one and a non-stiff one. The two considered axial stiffnesses are reported in Table 4 and refer to two different materials: an aramid fiber for the stiff case and polyethylene for the non-stiff case.

Results on relative distance between the two bodies and tension evolution on the tether are shown in Fig. 17 for the stiff case and Fig. 18 for the non-stiff case. In these figures the first 920 s refer to the burn phase while the final time span refers to the post-burn/free motion phase (even if the tether is already supposed to be cut after the engines shutting down).

In Fig. 17, the high frequency oscillations are due to the high material stiffness. After the burn the tether slackens and the two object are pulled closer, the closer approach being under 20 m of distance between the centers of mass.

It is important to remark that a millimeter diameter synthetic fiber can withstand this level of stress: in fact high modulus – high strength fibers such as Kevlar or Dyneema, meets the required mechanical and thermal properties. According to this, a low damping ($\sim$0.3) has been assumed.

In Fig. 18, the same figures are reported for the non-stiff tether case. Here the tether behavior as a spring is evident: during the burn phase the system oscillates with lower frequency and higher amplitude with respect to the case above. After the burn, if the tether is not cut, the bodies continue to dangerously oscillate around the system center of mass, continually stretching and releasing the tether. Furthermore amplitude and frequency trends of this phase are strongly affected by control parameters and system states at the end of the burning phase.

Even if lower frequency is attractive from a control point of view, having tether tension as feedback, it is evident from Figs. 19 and 20 how such high amplitude oscillation is unattractive from the controllability and safety point of view. A non-stiff tether makes the chaser attitude more difficult to control and the drift from velocity direction alignment is bigger, meaning less transfer efficiency.

The tether contact point is slightly misaligned with the target center of mass, due to the presence of appendages: this means that the tether also exchanges a torque with the connected body. The target angular momentum builds up, because of tether axial oscillations, leading, in the case of a non-stiff tether, to instability of target angular motion and possible entanglement.

4.2. Post-burn control recovery

If a multi-burn strategy is foreseen, it is necessary to recover control at the end of each burn. A simple PID controller has been implemented to preliminary demonstrate

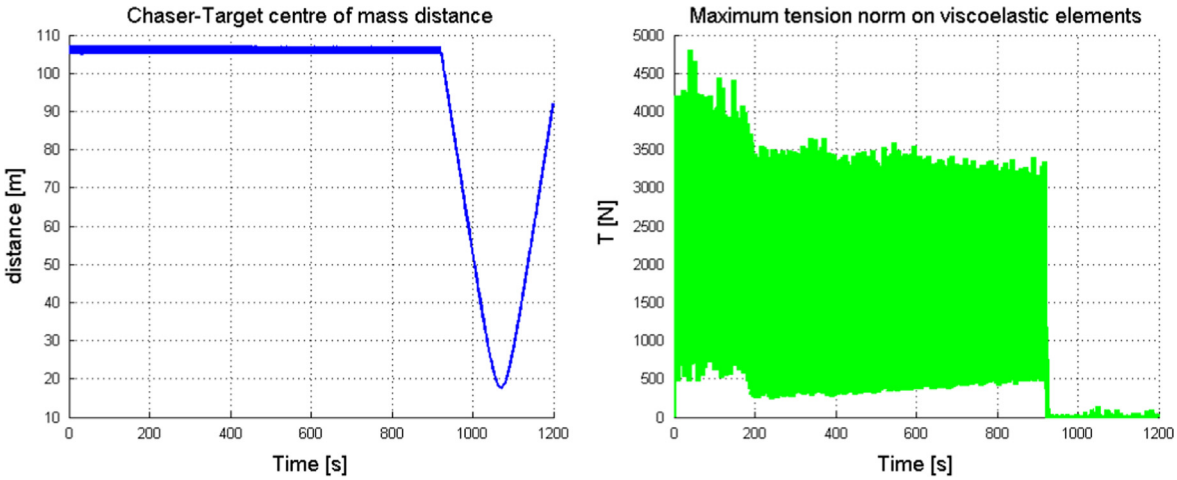

Fig. 17. Chaser-target distance and tether tension evolution – stiff case.

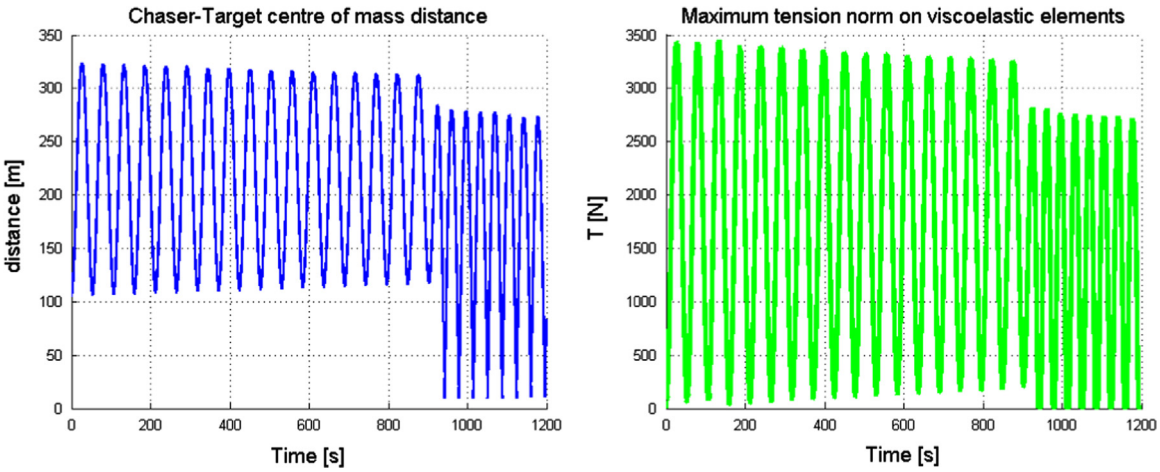

Fig. 18. Chaser-target distance and tether tension evolution – non-stiff case.

the feasibility of control recovery. Controller feedback is the relative position between bodies and the tether tension: the main burn is stopped when the tension is minimum and then the reaction control system of the chaser (here supposed to have a maximum authority of 100 N) are fired to keep the chaser in the desired relative position with respect to the target. The simulation parameters are the ones reported in Table 3; the stiff tether case is here analyzed.

In Fig. 21 the relative distance is reported, focusing on the end of the burn: the minimum distance achieved between the bodies is now above 90 m. The chaser is able to recover the nominal relative position, however multiple firings are necessary to counteract the tether tensioning and following release. Further improvement will see the refinement of control laws to significantly damp the oscillations around the nominal position and the insertion of reel control on tether tension, to avoid multiple burns with the reaction control system.

During pulling, the system orbital eccentricity increases and the altitude of perigee decreases: the orbit gets more and more elliptical and the system orientates with the tether "crossing" the trajectory of the center of mass. This configuration implies an angle between the anti-velocity direction and the tether, leading to thrust losses that can be limited with a multi-burn de-orbiting. With this strategy several burns are made at the apogee, reducing the altitude of perigee, and between them the control is recovered after burn and the system is kept stable along *V*-bar: this is possible as long as the altitude does not reach the atmospheric interface, below which the control authority is not guaranteed. A final burn is given to set the system in the correct steep re-entry path: the maneuver synchronization with Earth rotation allows sea landing on a safe oceanic window.

5. Conclusion

Active debris removal is a challenging task for an automatic space vehicle for different reasons dealing with proximity maneuvers, non-cooperative targets and orbit displacement. A tethered-net system could provide an effective solution to this challenge: the tethered-net device, as it is conceived, it allows to capture medium/large size debris, to firmly and safely close around them, and to perform disposal. Precise numerical modeling and

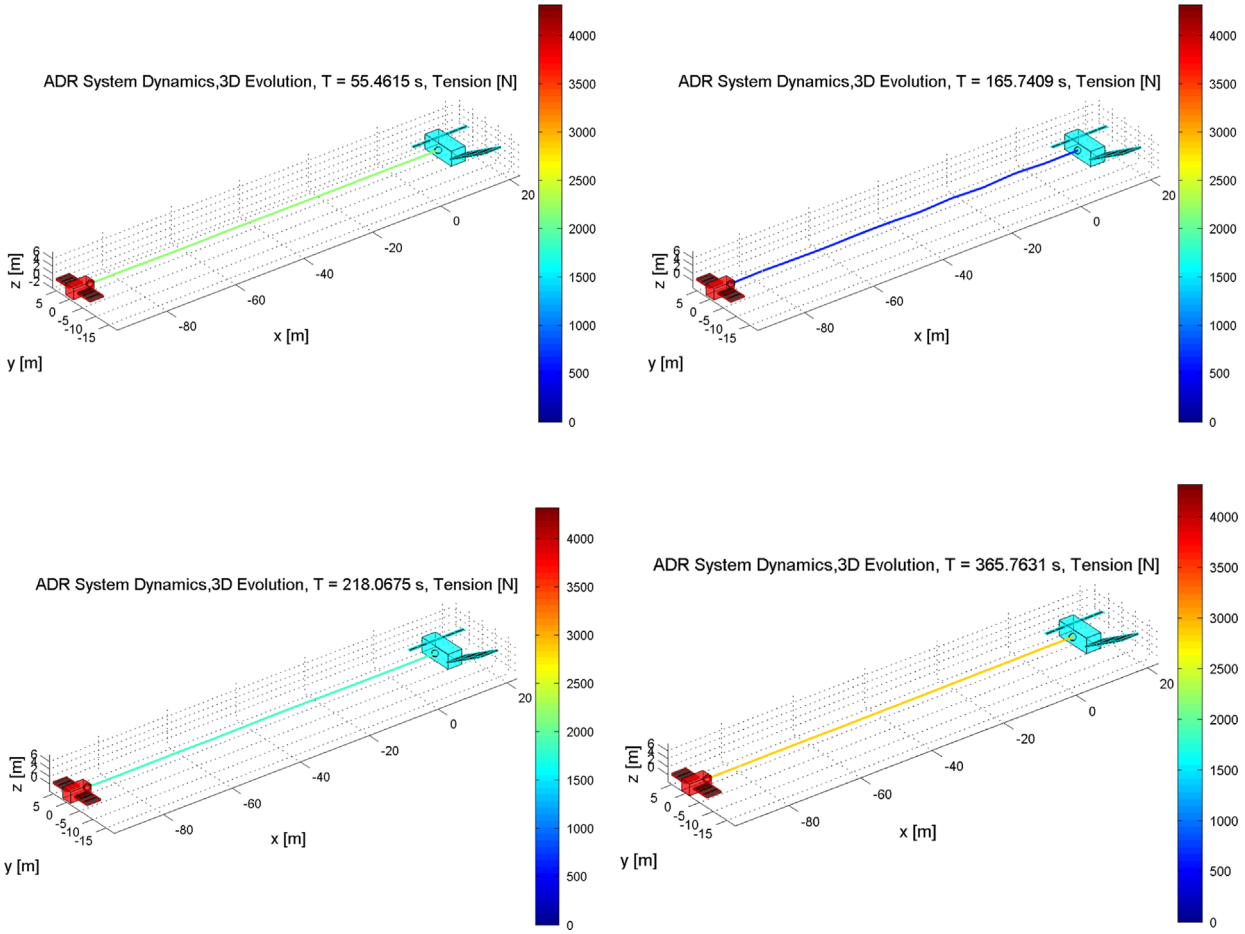

Fig. 19. System evolution in center of mass LVLH frame – stiff case.

GNC design is a challenging task for such systems. The beads model represents the best compromise between fast and accurate, allowing numerically stable simulations, faster management of variables and collision detection, an arbitrary discretization of the problem and the parallelization of the code. The developed multi-body dynamics simulator is very flexible in dealing with different scenarios and configurations (different bodies' properties, different net and mesh sizes and shapes, different initial conditions etc.); it also allows to treat different materials in a parametric way. Such a simulator allowed to assess the capture technique feasibility, to drive the system design and to support the GNC design.

Numerical simulations results have shown the possibility of using throw-nets and tow-tethers for space debris active removal. Net deployment simulations have shown that net shot epoch needs to be synchronized with target relative motion and attitude and that a closure around the target body needs to be assured to avoid the net slipping off. The spatial motion of the target has been considered for different system's parameters, showing the conditions under which it is possible to keep the system controllable during the pulling phase. Slackness of the tether can lead to tangling due to the high amplitude of the oscillations of the passive satellite relative to the tether: for target safe transportation, tether slackness should be avoided. It has been proved that the amplitude of stack oscillation primarily depends on the tether properties: a stiffer tether is preferred to reduce these critical oscillations. If a single burn mission was selected, the straightest solution would be to cut the cable immediately after the pulling phase and perform a collision avoidance maneuver. On the other side, if a multi-burn de-orbiting strategy needs to be carried out it is necessary to recover control and avoid collision between the two crafts at the end of the burning phase: either the thrust can be throttled or the burning time can be synchronized with the relative motion so that, at the end of a burn, zero relative velocity between the two connected bodies is achieved. In the last case, a feedback control is necessary because zero relative velocity is hardly achievable in reality; the control needs to be very reactive and the system response is very fast. The model used for de-orbiting assessment is simplified, being a single non-slipping contact point considered. This is not completely representative of a net capturing where multiple slipping contact points are present, but it allowed to preliminary demonstrate the feasibility and size the system.

Current work, carried out at PoliMi-DAST, sees the refinement of control laws and the insertion of feedback control on tether tension using reel control, the model refinement and the insertion of perturbation, as air drag,

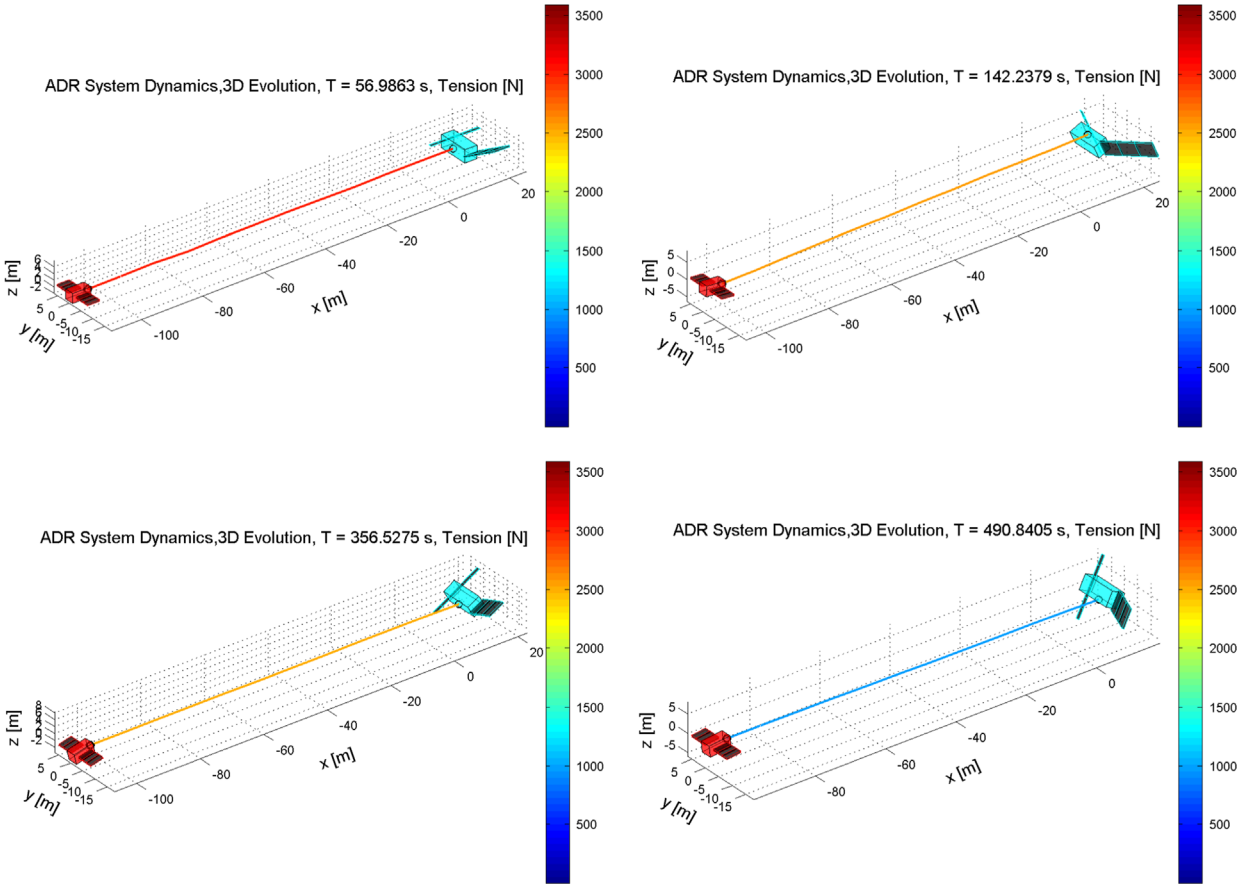

Fig. 20. System evolution in center of mass LVLH frame – non-stiff case.

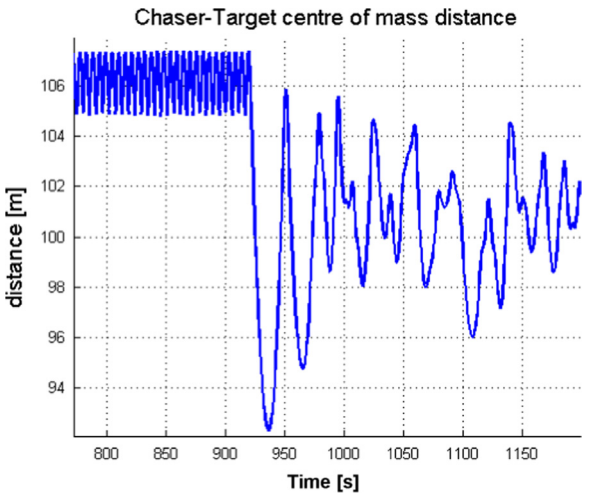

Fig. 21. Relative distance between chaser and target centers of mass at the end of the burn – post-burn control recovery.

supposed to play an important role in de-orbiting missions. The influences on the pulling phases are being evaluated for multiple slipping contact points instead of a single and fixed one: the net deployment model is currently being integrated with the de-orbiting model to simulate all mission phases within a single reliable simulation environment. The final goal is the implementation of the whole GNC loop and its robustness proof, as well as the design of the tethered-net payload.

Finally, an effort is also being put in validating the developed models: first validations have already been performed through benchmarking with analytical results and on-ground experiments. A microgravity experimental campaign has been scheduled to validate dynamics models in a relevant environment.

Acknowledgements

The authors acknowledge the European Space Agency TEC-ECN and TEC-MMA divisions for supporting studies related to the topic here discussed.

Appendix A. Dynamics Models and Equations of Motion

Within the net deployment dynamics the following references frames are defined

- Earth Centered Inertial (ECI), centered in the Earth
  - **1-axis** permanently fixed towards the vernal equinox;
  - **2-axis** in the Earth equatorial plane, right-hand side orthogonal 1–3;

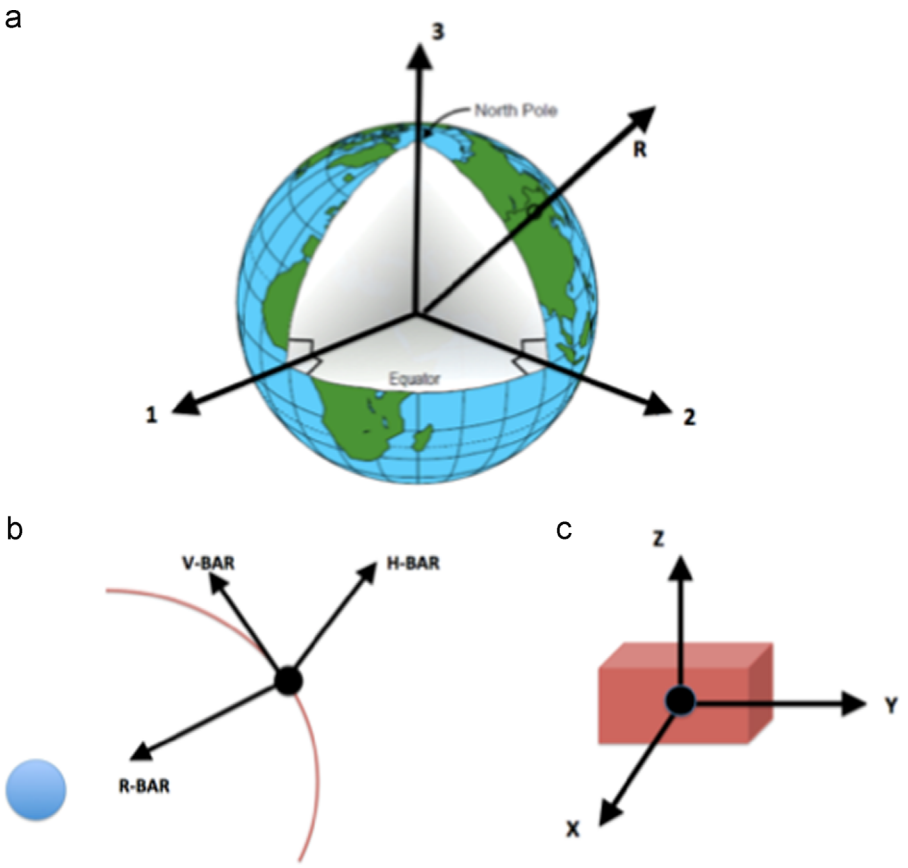

Fig. 22. Reference frames: (a) ECI, (b) LVLH, (c) BODY.

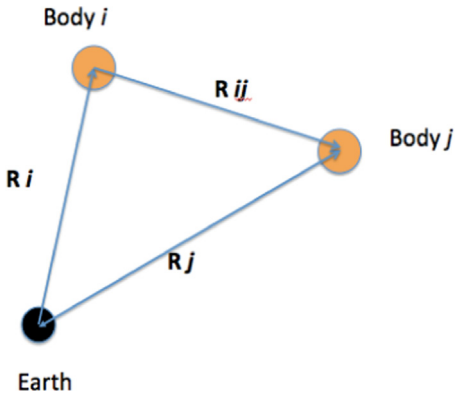

Fig. 23. Relative position convention.

  - **3-axis** lies at a 90° angle to the equatorial plane and extends through the North Pole.
- Local Vertical–Local Horizontal reference frame (LVLH), centered in the system center of gravity
  - ***H*-bar** axis opposite to the angular momentum of the orbit;
  - ***R*-bar** axis towards the main attractor;
  - ***V*-bar** transverse axis (along the target velocity direction if circular orbit), orthogonal to *H*–*R*.
- Body reference frame, (BODY) centered in the body center of mass, the axis definition, ***X*-axis**, ***Y*-axis,** ***Z*-axis**, depending on the body inertia matrix definition *I*.

These reference frames are represented in Fig. 22.

Vectors, quaternions and matrix are written here in bold characters. Each body center of mass coordinate system is defined with respect to the ECI frame called world: any physical variable expressed with respect to this frame is referred as an absolute and indicated with a capital letter; for example $\boldsymbol{R_i}$ and $\boldsymbol{V_i}$ are the position and velocity vectors of body *i* in ECI frame. On the other hand, quantities referred to BODY coordinate system are indicated with a lowercase letter: for example $\boldsymbol{r_i}$ is the position an of point *i* in BODY frame. Double indexes indicate relative distance between two points: for example, $\boldsymbol{R_{ij}} = \boldsymbol{R_j} - \boldsymbol{R_i}$, is the relative position vector expressed in ECI frame between body *i* and *j*, pointing from *i* com towards *j* com as represented in Fig. 23.

Rigid body kinematics is described by rotation quaternions. A quaternion is defined as

$$\boldsymbol{q} = \begin{Bmatrix} v_1 \\ v_2 \\ v_3 \\ s \end{Bmatrix} = \begin{Bmatrix} e_1 \sin\frac{\theta}{2} \\ e_2 \sin\frac{\theta}{2} \\ e_3 \sin\frac{\theta}{2} \\ \cos\frac{\theta}{2} \end{Bmatrix} \tag{9}$$

where the last element is defined as the scalar part or real part, representing the cosine term of the rotation angle, and the first 3 elements represent the vector part (vector v) or imaginary part. A vector transformation from frame A to frame B, by means of the rotation quaternion, is performed with the following equation

$$\begin{bmatrix} 0 \\ \boldsymbol{v_B} \end{bmatrix} = \boldsymbol{q_{BA}} \begin{bmatrix} 0 \\ \boldsymbol{v_A} \end{bmatrix} \boldsymbol{q^*_{BA}} \tag{10}$$

where

- $\boldsymbol{v_A}$ is a vector in the frame A;
- $\boldsymbol{q_{BA}}$ is the quaternion from frame A to frame B;
- $\boldsymbol{q^*_{BA}}$ is the conjugate of $\boldsymbol{q_{BA}}$;
- $\boldsymbol{v_B}$ is the vector in the frame B.

As a quaternion represents a rotation from one frame to another frame, the quaternion multiplication can multiply this kind of frame transformations, as expressed by the following:

$$\boldsymbol{q_{CA}} = \boldsymbol{q_{CB}} \boldsymbol{q_{BA}} \tag{11}$$

where

- $\boldsymbol{q_{CA}} = \boldsymbol{q_{A\to C}}$ is the quaternion from frame A to frame C;
- $\boldsymbol{q_{CB}} = \boldsymbol{q_{B\to C}}$ is the quaternion from frame B to frame C;
- $\boldsymbol{q_{BA}} = \boldsymbol{q_{A\to B}}$ is the quaternion from frame A to frame B.

The adopted convention is

- $\boldsymbol{q_{absolute}}$ is the quaternion from ECI frame to BODY frame;
- $\boldsymbol{q_{oribital}}$ is the quaternion from ECI frame to LVLH frame;
- $\boldsymbol{q_{attitude}}$ is the quaternion from LVLH to BODY.

Therefore

$$\boldsymbol{q_{absolute}} = \boldsymbol{q_{attitude}} \boldsymbol{q_{orbital}} \tag{12}$$

Newton's equations of dynamics are described in ECI frame, in order not to model fictitious forces. Euler's equations are derived in body frame, instead. The gravitational forces and torques are applied to each body independently, depending on its absolute position and attitude. Torques are not applied to point masses for obvious reasons: rotational dynamics are not described for point masses.

The gravitational force, acting on body (or element) *i*, is defined as

$$\boldsymbol{F_{Gi}} = -\frac{\mu m_i}{|\boldsymbol{R_i}|^3} \boldsymbol{R_i} \tag{13}$$

where

- μ is the gravitational constant;
- m_i is the element mass *i*
- $\boldsymbol{R_i}$ is the vector position of element *i* in ECI frame.

The gradient gravity torque is given for mass *i* as per the following equation:

$$\boldsymbol{M_{Gi}} = -\frac{3\mu}{|\boldsymbol{R_i}|^3} \boldsymbol{c_i} \times \boldsymbol{I_i} \boldsymbol{c_i} \tag{14}$$

where $\boldsymbol{I_i}$ is the inertia matrix of body *I* and $\boldsymbol{c_i}$ is the vector of the direction cosines of the radial position of the body *i* com expressed in body axis as as per the following equation:

$$\boldsymbol{c_i} = \frac{\boldsymbol{r_i}}{|\boldsymbol{r_i}|} \tag{15}$$

Chaser, target and bullets

Target and chaser are parallelepiped bodies defined by

- mass *M* and inertia $\boldsymbol{I}$;
- three linear dimensions in BODY frame [*a,b,c*];
- tether connection point expressed in BODY frame;
- initial position $\boldsymbol{R_o}$, velocity $\boldsymbol{V_o}$, angular velocity $\boldsymbol{\omega_o}$ and orientation $\boldsymbol{q_o}$ wrt ECI frame.

The target is non-cooperative and uncontrolled while the chaser can be controlled. In the following equations, the subscript *T* refers to the target, while *C* to the chaser.

The non-linear dynamics of the target is given in the following equations :

$$M_T \frac{d^2 \boldsymbol{R_T}}{dt^2} = \boldsymbol{F_{GT}} + \boldsymbol{F_C} + \boldsymbol{F_{ext}} + \sum_{i=1}^{NFA} \boldsymbol{F_{FAi}} \tag{16}$$

$$\boldsymbol{I_T} \dot{\boldsymbol{\omega}}_{\boldsymbol{T}} + \boldsymbol{\omega_T} \times \boldsymbol{I_T} \boldsymbol{\omega_T} = \boldsymbol{M_{GT}} + \boldsymbol{M_C} + \boldsymbol{M_{ext}} + \sum_{i=1}^{NFA} \boldsymbol{M_{FAi}} \tag{17}$$

where

- M_T, $\boldsymbol{R_T}$, $\boldsymbol{I_T}$, $\boldsymbol{\omega_T}$ are respectively target mass, center of gravity position in ECI frame, inertia matrix and angular velocity in BODY frame;
- $\boldsymbol{F_{GT}}$ and $\boldsymbol{M_{GT}}$ are the gravitational forces acting on target as expressed in Eqs. (13) and (14);
- $\boldsymbol{F_C}$ and $\boldsymbol{M_C}$ are the contact force and torque acting on target, as a result of the sum of contribution of each element of the target mesh;
- $\boldsymbol{F_{FAi}}$ and $\boldsymbol{M_{FAi}}$ are reaction forces and torques of flexible appendage *i*, being *NFA* the number of flexible appendages connection points,
- $\boldsymbol{F_{ext}}$ and $\boldsymbol{M_{ext}}$ are external forces and torques given by external inputs (for example perturbations).

The equations of motion for the chaser are given by

$$M_C \frac{d^2 \boldsymbol{R_C}}{dt^2} = \boldsymbol{F_{GC}} - \boldsymbol{T}_{12} + \boldsymbol{F_{ext}} + \sum_{i=1}^{NFA} \boldsymbol{F_{FAi}} \tag{18}$$

$$\boldsymbol{I_C} \dot{\boldsymbol{\omega}}_{\boldsymbol{C}} + \boldsymbol{\omega_C} \times \boldsymbol{I_C} \boldsymbol{\omega_C} = \boldsymbol{M_{GC}} + \boldsymbol{M}_{T12} + \boldsymbol{M_{ext}} + \sum_{i=1}^{NFA} \boldsymbol{M_{FAi}} \tag{19}$$

where, obvious terms, $\boldsymbol{T}_{12}$ and $\boldsymbol{M_T}_{12}$ are the reaction force and torque exercised by the tether on the chaser, as defined in Eqs. (1) and (21).

Bullets are cylindrical rigid bodies defined by their mass, inertia and net connection point. Their motion is described by six scalar equations, as Eqs. (18) and (19), not repeated here, where reactions due to elements in tension are taken

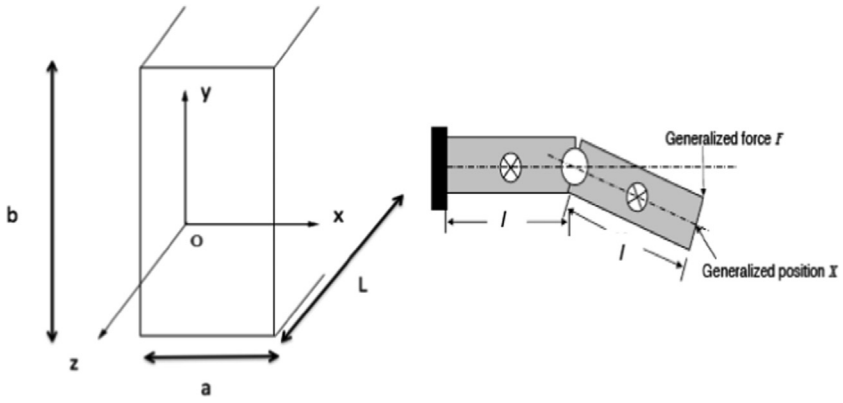

Fig. 24. Beam reference frame and conventions.

into account for all the connected threads and connection points, if multiple connections are applicable. Bullets have time varying mass depending on the length variation and consequent mass variation of closing threads.

5.1. Tether and net

Cables and ropes, such as the tether and net, are modeled with the lumped-parameter method, also called beads model. Tether/net ropes are defined by

- rope length L_T;
- rope diameter D_T;
- Young modulus E_T;
- damping coefficient d_T;
- material density ρ_T;
- n number of discretization elements.

The length of each rope is supposed to have a fixed length during forward dynamics propagation, except for closing threads whose properties are time varying (mass, stiffness and damping depending on the actual user-controlled length).

The tether is discretized with n_T point masses, nominal length between two masses $l=L_T/n_T$ and equal mass $m_i=m_T/n_T$, connected by spring-dampers, Eq. (1), that can only exchange axial forces under tension (no forces exchanged under compression).

The equations of motions for masses $i=[2\text{–}n]$ are given by

$$m_i\frac{d^2\boldsymbol{R_i}}{dt^2}=\boldsymbol{F_{Gi}}+\sum_{j=-1,1}\boldsymbol{T}_{i,i+j}+F_{Ci}+F_{exti} \tag{20}$$

and for the first mass it is

$$m_1\frac{d^2\boldsymbol{R}_1}{dt^2}=\boldsymbol{F_{G1}}+\boldsymbol{T}_{12}+F_{C1}+F_{ext1} \tag{21}$$

where, a part from terms already defined above, it is

- $\boldsymbol{T}_{T\,i,i+j}$ is the tension between the mass i and $i+j$, depending on their relative position and velocities as detailed in Eqs. (1)–(3);
- $\boldsymbol{F_{Ci}}$ is the contact force acting on each bead of the tether.

In a general net configuration, the Newton's equation for a mass m_i ($i=1$ to total number of net knots) is given by

$$m_i\frac{d^2\boldsymbol{R_i}}{dt^2}=\boldsymbol{F_{Gi}}+\sum_{j=l}\boldsymbol{T}_{i,i+j}+\boldsymbol{F}_{ext} \tag{22}$$

where $j=l$ is the index number of all masses connected through an element rope to that knot i.

Flexible appendages

Flexible appendages are modeled with a lumped-parameter method, as a chain of extended (6 degrees of freedom, non-null inertia) rigid bodies and viscoelastic joints. Flexible appendages are defined by

- beam length L_{FA} along local z-axis and dimensions a_{FA}, b_{FA} along local x and y axis (Fig. 24);
- beam mass m_{FA} and inertia matrix;
- Young modulus E_{FA};
- damping coefficient d_{FA};
- n number of discretization element;

The beam is discretized with n rigid body elements, each of length $l=L_{FA}/n$ and mass $m=m_{FA}/n$, with the element com at l/2 along the beam axis, divided by viscoelastic joints that can exchange axial forces and bending torques computed as:

$$\boldsymbol{F}_{FA}=(-k_{ax}\Delta z-d_{FA}\Delta\dot{z})\hat{\boldsymbol{z}} \tag{23}$$

$$\boldsymbol{M}_{FA}=(-k_{flex,x}\,\Delta\theta_x-d_{FA}\Delta\dot{\theta}_x)\hat{\boldsymbol{x}}+(-k_{flex,y}\,\Delta\theta_y-d_{FA}\Delta\dot{\theta}_y)\hat{\boldsymbol{y}} \tag{24}$$

with

$$k_{ax}=\frac{EA}{l} \tag{25}$$

$$k_{flex,x}=\frac{EJ_{xx}}{l}\ \text{and}\ k_{flex,y}=\frac{EJ_{yy}}{l} \tag{26}$$

being $A=a_{FA}\,b_{FA}$, $J_{xx}=a_{FA}\,b_{FA}^3/12$ and $J_{yy}=b_{FA}\,a_{FA}^3/12$.

Here, twisting around the beam axis has not been considered: its integration into the model is immediate, given the considerations above, introducing shear modulus G_{FA} and

by considering

$$k_{twist} = \frac{G_{FA}J}{l} \tag{27}$$

where $J = J_{xx} + J_{yy}$.

By defining $\boldsymbol{X}$ and $\boldsymbol{F}$ as the generalized coordinates and forces, respectively, at the tip of the beam (as in Fig. 24) and $\boldsymbol{x}$ as the parameterization of the degrees of freedom of the joint. Then

$$\boldsymbol{X} = \boldsymbol{g}(\boldsymbol{x}) \quad \text{and} \quad \boldsymbol{dX} = \boldsymbol{J}(\boldsymbol{x})\boldsymbol{dx} \tag{28}$$

where $\boldsymbol{J}(\boldsymbol{x}) = \frac{\delta g(\boldsymbol{x})}{\delta x}$ is the Jacobian. The generalized force $\boldsymbol{F}$ at the tip can be expressed with a generalized stiffness matrix $\boldsymbol{K}$

$$\boldsymbol{F} = \boldsymbol{K}\boldsymbol{dX} \tag{29}$$

while the generalized force $\boldsymbol{f}$ at the joint can be expressed as

$$\boldsymbol{f} = \boldsymbol{k}\boldsymbol{dx} \tag{30}$$

where $\boldsymbol{k}$ is the equivalent spring constant at the joint of a generalized beam elements and $\boldsymbol{dx}$ is the infinitesimal generalized relative displacement between the two bodies across the joint. It is easy to demonstrate by energetic approach that

$$\boldsymbol{k} = \boldsymbol{J}^{\boldsymbol{T}} K J \tag{31}$$

being $\boldsymbol{k}$ composed by the terms expressed above in Eqs. (25)–(27).

The reactions forces and torques of the flexible appendages on the body are the generalized forces/torques calculated at the interface and depend on the interface (or joint) element: in the generalized case it is

$$F_{reaction} = \boldsymbol{f}(z = 0) \tag{32}$$

References

[1] J.C. Liou, N.L. Johnson, A sensitivity study of the effectiveness of active debris removal in LEO. in: Proceedings of the 58th International Astronautical Congress, IAC-07-A6.3.05, Hyderabad, India, 2007.

[2] K. Wormnes, R. Le Letty, L..Summerer, R. Schonenborg, O. Dubois-Matra, E. Luraschi, A. Cropp, H. Krag and J. Delaval, ESA technologies for space debris remediation. in: Proceedings of the 6th European Conference on Space Debris, Darmstadt, 2013.

[3] K. Wormnes, J.H. de Jong, H. Krag, G. Visentin, Throw-nets and tethers for robust space debris capture. in: Proceedings of the 64th International Astronautical Congress, IAC-13, Beijing, China, 2013, A6.5, 2 × 16445.

[4] S. Hobbs, Debris removal from low Earth orbit DR LEO (College of Aeronautics Report 1001), Cranfield University, UK, 2010.

[5] S. Nishida, T. Yoshikawa, Space debris capture by a compliance controlled robot, , in: Proceeding of the IEEE/ASME National aerospace laboratory of Japan 2003.

[6] Astrium, RObotic GEostationary orbit Restorer (ROGER) Phase A Final Report, ROGSIBRE- FP Issue 1, 26 June 2003.

[7] R. Biesbroek, The e.Deorbit study in the concurrent design facility, presentation handouts, in: Proceedings of the Workshop on Active Space Debris Removal, 17 September 2012.

[8] E. Kim, R. Vadali, Modeling issues related to retrieval of flexible tethered satellites systems, J. Guid. Control Dyn. 18 (5) (1995) 1169–1176.

[9] C. Lee, B. Cha, H. Kim, Physical modeling for underwater flexible systems dynamic simulation, Ocean Eng. (2005) 331–347. (October).

[10] K. Suzuki, T. Takagi, T. Shimizu, T. Hiraishi, K. Yamamoto and K. Nashimoto, Validity and visualization of a numerical model used to determine dynamic configurations of fishing nets Fish. Sci. 2003; 69: 695–705, January 2003.

[11] P. Williams, Dynamic multibody modeling for tethered space elevators, Acta Astronaut. 65 (399–422) (2009) 399–422.

[12] V.S. Aslanov, A.S. Ledkov, Dynamics of Tethered Satellite Systems, Woodhead, Oxford, 2012.

[13] M.J. Leamy, A.K. Noor, T.M. Wasfy, Dynamic simulation of a tethered satellite system using finite elements and fuzzy sets, Comput. Methods Appl. Mech. Eng. 190 (37–38) (2001) 4847–4870.

[14] W. Fluggë, Viscoelasticity, Blaisdell, Waltham, MA, 1967.

[15] L. Shampine, M. Hosea, Analysis and implementation of TR-BDF2, Appl. Numer. Math. 20 (1996) 21–37.

[16] V. Chudnovsky, et al., Modeling Flexible Bodies in SimMechanics and Simulink, Matlab Digest, US, 2006 (May).

[17] G. Zachmann, Virtual Reality in Assembly Simulation – Collision Detection, Simulation Algorithms and Interaction Techniques, Department of Computer Science, Darmstadt University of Technology, 2000 (Ph.D. thesis).

[18] M. Woulfe, M. Manzke, A Framework for Benchmarking Interactive Collision Detection, Trinity College Dublin, Budmerice, Slovakia, April 2009.

[19] P.M. Hubbard, Approximating Polyhedra with Spheres for Time-Critical Collision Detection, ACM Trans. on Graphics, USA, 1996.

[20] I.J. Palmer, R.L. Grimsdale., Collision Detection for Animation Using Sphere-Trees, Computer Graphics Forum, UK, 1995 (June).

[21] G. Barequet, B. Chazelle, L. Guibas, J. Mitchell, A. Tal. BOXTREE: a hierarchical representation for surfaces in 3D, in: Proceedings of Eurographics, Computer Grapics Forum 1996.

[22] G. Hippmann, An Algorithm for Compliant Contact Between Complexly Shaped Surfaces in Multi-Body Dynamics, Institute of Aeroelasticity DLR – German Aerospace Center, Wessling, Germany.

[23] R. Janovsky, et al., End-of-Life De-Orbiting Strategies for Satellites, OHB System AG Bremen, Germany, 2002 (DGLR-JT).

[24] L.Z. Jasper and H. Schaub, Input shaped large thrust maneuver with a tethered debris object, in: Proceedings of the 6th European Conference on Space Debris, Aerospace Engineering Sciences Department, University of Colorado, USA , Darmstadt, 2013.